COBEM 2021 26th International Congress of Mechanical Engineering
ABCM Associação Brasileira de Engenharia e Ciências Mecânicas
November 22-26, 2021, Virtual Congress, Brazil

COB-2021-0716
ROBUST DESIGN OF ENERGY HARVESTING RESONANT DEVICES BY MULTI-OBJECTIVE OPTIMIZATION TECHNIQUES AND POLYNOMIAL CHAOS EXPANSIONS

Paulo H. Martins
Marcelo A. Trindade
Paulo S. Varoto
São Carlos School of Engineering, University of São Paulo, SP 13566-590, Brazil
paulo.martins@usp.br, trindade@sc.usp.br, varoto@sc.usp.br

Abstract. *In recent years, energy harvesting from mechanical vibrations has been a very active research topic. This can be achieved with help of piezoelectric materials which can be used to convert mechanical energy into electricity. This is particularly interesting to energize moving or portable devices, which still rely heavily on batteries. Nevertheless, the amount of energy available for conversion is usually small and the conversion efficiency is highly sensitive to uncertainties found in the harvesting devices themselves and their environment. Thus, the design of energy harvesting devices should account for uncertainty analysis and robust optimization techniques. This work presents some recent results on the robust design of energy harvesting devices, based on cantilever resonating beams, when subjected to uncertainties on the beam clamping, harvesting circuit and effective damping. Multi-objective optimization techniques are considered to search for optimal values of design parameters, namely beam length, piezoeletric patch length, position and thickness and circuit effective resistance, leading to satisfactory compromises between mean and dispersion of the potentially harvested energy. Due to the high computational cost of uncertainty quantification, estimation of mean and dispersion of the response is found using Polynomial Chaos Expansions (PCE) and two multi-objective techniques are considered, Compromise Programming (CP) and Non-dominated Sorting Genetic Algorithm (NSGA-II). Results show that harvesting devices with smaller length and larger masses generally lead to best nominal performance but also to higher dispersions. Also, the dispersions can be reduced by using effective circuit resistances smaller than the nominal values. Several design alternatives are presented in the form of a Pareto front, from which a designer can choose based on the desired compromise.*
Keywords: *energy harvesting, piezoelectric materials, uncertainties, optimization, robust analyses*

1. INTRODUCTION

Research on energy harvesting from mechanical vibrations has been very active in recent years, since increasing energy consumption has been motivating the search for alternative energy sources and energy harvesting devices can be designed using piezoelectric materials to convert vibratory energy into electricity. Piezoelectric materials are able to generate electrical charges when deformed and, thus, can be used as strain sensors (Leo, 2007). Using specific electrical circuits connected to the piezoelectric sensor electrodes allows to capture the energy generated by the device motions. A popular energy harvesting device is based on a cantilever beam designed to resonate when subjected to base excitation at the clamping, which is to be attached to the moving source. When the cantilever beam resonates, a piezoelectric material attached to it deforms and induces electrical charges that can be captured by an especially designed electrical circuit. The power generated by device can be calculated using a Frequency Response Function (FRF), which maximum value happens when the excitation and device resonance frequencies are the same. Thus, a tip mass is generally used to tune the device resonance frequency to the excitation one. Fig. 1 shows a typical model of energy harvesting devices based on resonating cantilever beams which is composed of a substrate with an effective length l_v, a tip mass m_b with a portion of the beam underneath and with length l_b, a piezoelectric patch adhesively bonded to the substrate, an electrical resistance R_c, aimed at representing the harvesting electrical circuit, and a clamp subjected to a displacement $w_0(t)$, coming from the moving source to which the harvesting device is attached to.

Different approaches have been used for the modeling of such piezoelectric energy harvesters, such as single degree of freedom models (Dutoit *et al.*, 2005), distributed parameters models (Erturk and Inman, 2011), Raleigh–Ritz models (Kim *et al.*, 2010) and finite element models (Godoy and Trindade, 2012; Godoy *et al.*, 2014; De Marqui Junior *et al.*, 2009). Regardless of the chosen approach, optimization methods are essential for designing suitable devices since the output energy is both small and a complex function of the input parameters. Optimization methods seek to find an optimal solution by minimizing/maximizing an objective function that may be subject to constraints (Rao, 2009). Modern or nontraditional optimization techniques based on metaheuristic algorithms, such as ant colony, simulated annealing, neural

networks and genetic algorithms, generally find the optimal solutions or values in the vicinity of these targets with the advantage of being able to tackle complex engineering problems, such as non-convex problems.

Although optimization techniques can be used to find satisfactory nominal solutions for energy harvesting problems, it is important to consider the presence of uncertainties to design devices that could be effective in real conditions. For this reason, research has been carried out by considering energy harvesting devices with uncertainties in the parameters or in the environment (Godoy and Trindade, 2012; Franco and Varoto, 2017; Kim *et al.*, 2017; Lee and Park, 2006; Ruiz and Meruane, 2017). In the case where devices are designed to become less sensitive to uncertainties, the design is known as robust design and the methodology as robust design optimization (Schuëller and Jensen, 2008). An alternative for finding robust designs is to estimate the mean, variance and/or a sensitivity function of the response, and search for a trade-off between one of these last two functions and the mean (Beyer and Sendhoff, 2007). The main challenge of estimating the mean and variance is to find a specific procedure with a satisfactory computational cost. For instance, Monte Carlo Simulation (MCS) can be used but the computational cost is generally too expensive to include in optimization schemes. Alternative methods have been proposed to solve these issues, such as approximations using Taylor series, Karhunen–Loève and polynomial chaos expansions, as well as using surrogate models in substitution of the original model (Beyer and Sendhoff, 2007; Lee and Park, 2006; Schuëller and Jensen, 2008). Since two objectives should be accounted for, mean and variance, multi-objective optimization strategies should be employed to find a satisfactory compromise between the nominal performance and its variability or robustness.

The choice of the multi-objective optimization strategy depends on the problem and there are a number of existing alternatives (Marler and Arora, 2004; Lobato, 2008). The traditional weighted sum strategy, to transform a multi-objective problem into a mono-objective one, is easier to use and apply, but the solutions cannot be reached for non-convex or discontinuous problems. On the other hand, a mathematical formulation for bi-objective robust design (BORD) known as Compromise Programming (CP) can solve non-convex problems when optimization methods are used to search for an ideal solution (Chen *et al.*, 1998). Generally, the multi-objective optimization methods find numerous solutions which are presented in a curve known as Pareto front, from which the decision-maker may choose an appropriate solution based on any specific criteria. For that, it is important that the solutions are well distributed and that there is good diversity in the Pareto front. The CP method uses a weighting factor which can be modified resulting in different points in the Pareto front and from which the decision-maker may obtain the required weighting factor for a specific solution. Furthermore, metaheuristic methods can be used to optimize a multi-objective problem since many solutions are generated and the choice is made a *posteriori*. Some of these methods are inspired in nature or based on the evolution, such as multi-objective particle swarm optimization and genetic algorithm (Coello *et al.*, 2004; Deb *et al.*, 2002).

This work presents some recent results on the robust design of energy harvesting devices, based on cantilever resonating beams, when subjected to uncertainties on the beam clamping, harvesting circuit and effective damping. This is done using an electromechanical coupled finite element model combined to a modal reduction to evaluate the power output that could be harvested from a given device. Multi-objective optimization techniques are considered to search for optimal values of design parameters, namely beam length, piezoeletric patch length, position and thickness and circuit effective resistance, leading to satisfactory compromises between mean and dispersion of the potentially harvested energy. To cope with the high computational cost of uncertainty quantification, the estimation of mean and dispersion of the response is found using PCE and two multi-objective techniques are considered, CP and NSGA-II. The results obtained with the two optimization strategies are analyzed and compared in terms of both optimal solutions found and corresponding computational cost. Pareto fronts and box plots as supporting guides for decision-making are presented and analyzed.

2. FINITE ELEMENT MODEL OF A PIEZOELECTRIC ENERGY HARVESTING DEVICE

The model used for designing the devices is based on a finite element model with three layers developed in a previous work (Santos, 2008). Bernoulli-Euler theory is assumed for the surface (upper and lower) layers, while Timoshenko theory is assumed for the core (central) layer. Here, the core layer is used for the adhesive layer, thus, it is allowed to present shear strains. All layers are assumed to be perfectly bonded. For piezoelectric layers, linear piezoelectric orthotropic materials are considered with electrodes covering its upper and lower surfaces. The model is schematically presented in Fig. 2, where an imperfect clamp is simulated by using a combination of linear k_w and torsional k_θ springs coupled to the finite element node at the left (clamped) end, an electrical resistance R_c is connected to the piezoelectric patch, which is bonded to the substrate by an adhesive layer. Parameters l_p and h_p correspond to the length and thickness of the piezoelectric patch, that is bonded at a distance d_p from the clamp. l_v and h_v are the length and thickness of the substrate. A tip mass, represented by a rectangular cuboid with height h_b, length l_b and width b, is used to tune the fundamental resonance frequency of the device with that of the base excitation $w_0(t)$. The equations of motion are written as

$$\mathbf{M}_{rr}\ddot{\mathbf{u}}_r + \mathbf{K}_{rr}\mathbf{u}_r - \bar{\mathbf{K}}_{me}q_c = \mathbf{m}^\star\ddot{w}_0(t), \tag{1}$$

$$R_c\dot{q}_c - \bar{\mathbf{K}}_{me}^t\mathbf{u}_r + \bar{K}_e q_c = 0, \tag{2}$$

where $\mathbf{M}_{rr}$ is the mass matrix, $\mathbf{K}_{rr}$, $\bar{\mathbf{K}}_{me}$ and $\bar{\mathbf{K}}_{e}$ are the mechanical, electromechanical and dielectric stiffness matrices, respectively. The term $\mathbf{u}_r$ is a vector of displacements relative to the base displacement, $w_0(t) = \tilde{w}_0 e^{i\omega t}$, while q_c is the electric charge induced in the piezoelectric patch. $\mathbf{m}^\star$ is a column vector composed of mass terms.

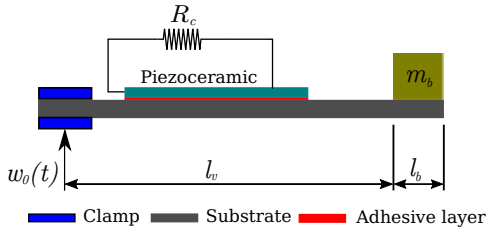

Figure 1: Typical model of energy harvesting devices based on resonating cantilever beams.

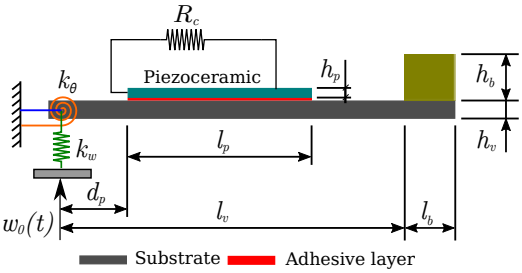

Figure 2: Schematic representation of the energy harvesting resonant device with imperfect clamp.

A model reduction using projection onto a truncated modal basis is performed, such that $\mathbf{u}_r \approx \boldsymbol{\phi}\boldsymbol{\alpha}_r$, where the modal basis is obtained from $[-\omega^2\mathbf{M}_{rr} + \mathbf{K}_{rr}]\boldsymbol{\phi} = 0$, considering $\mathbf{I} = \boldsymbol{\phi}^t\mathbf{M}_{rr}\boldsymbol{\phi}$ and leading to $\boldsymbol{\Omega}^2 = \boldsymbol{\phi}^t\mathbf{K}_{rr}\boldsymbol{\phi}$ and $\mathbf{K}_p = \boldsymbol{\phi}^t\mathbf{K}_{me}$. Moreover, a modal damping matrix $\boldsymbol{\Lambda}$ is included. Then, Eqs. (1) and (2) are rewritten as

$$(-\mathbf{I}\omega^2 + j2\omega\boldsymbol{\Lambda}\boldsymbol{\Omega} + \boldsymbol{\Omega}^2)\tilde{\boldsymbol{\alpha}}_r - \mathbf{K}_p\tilde{q}_c = \boldsymbol{\phi}^t\mathbf{m}^\star(-\omega^2\tilde{w}_0), \tag{3}$$

$$(j\omega R_c + \bar{K}_e)\tilde{q}_c - \mathbf{K}_p^t\tilde{\boldsymbol{\alpha}}_r = 0, \tag{4}$$

$\tilde{\boldsymbol{\alpha}}_r$ and $\tilde{q}_c$ correspond respectively to the modal displacements vector and electrical charge amplitudes.

Considering that the voltage output can be written as $V_c = R_c i_c$, where $i_c = \dot{q}_c$, and that Eqs. (3) and (4) can be solved for $\tilde{\boldsymbol{\alpha}}_r$ and $\tilde{q}_c$, it is possible to write the FRF for voltage output per unit base acceleration $G_{V\ddot{w}_0}(\omega) = \tilde{V}/(-\omega^2\tilde{w}_0)$ as

$$G_{V\ddot{w}_0}(\omega) = j\omega R_c\mathbf{K}_p^t\mathbf{D}^{-1}\boldsymbol{\phi}^t\mathbf{m}^\star, \tag{5}$$

where $\mathbf{D} = (j\omega R_c + \bar{K}_e)(-\mathbf{I}\omega^2 + j2\omega\boldsymbol{\Lambda}\boldsymbol{\Omega} + \boldsymbol{\Omega}^2) - \mathbf{K}_p\mathbf{K}_p^t$. Then, using the relation $P = V_c^2/R_c$, the FRF of power output per unit squared base acceleration $G_{P\ddot{w}_0}(\omega)$ is written as follows

$$G_{P\ddot{w}_0}(\omega) = (G_{V\ddot{w}_0}(\omega))^2/R_c. \tag{6}$$

This function can then be used to quantify the harvestable energy for a given set of design parameters and uncertain parameters. In the case of design parameters, this function can be directly evaluated for each parameters set. On the other hand, the values of uncertain (non-deterministic) parameters are not known a priori. If at least some information about the uncertain parameters are available, for instance mean and variance, it may be possible to construct a stochastic model for these parameters that could be used to quantify some statistics of the harvestable energy.

3. ESTIMATION OF OUTPUT MEAN AND VARIANCE

Using the polynomial chaos expansions (PCE), the mean and variance values of an output function can be determined, based on stochastic models for the input variables. The PCE is typically used to develop a stochastic metamodel to reduce the computational cost of evaluating the output function for a large number of realizations of the input variables. From a computational model $\mathcal{M}$ and a random vector $\mathbf{X}$, the response is defined as

$$Y = \mathcal{M}(\mathbf{X}). \tag{7}$$

This response can also be evaluated by PCE via the following procedure

$$Y = \sum_{\boldsymbol{\varrho}\in\mathbb{N}^M} c_{\boldsymbol{\varrho}}\Psi_{\boldsymbol{\varrho}}(\mathbf{X}), \tag{8}$$

where $c_{\boldsymbol{\varrho}}$ and $\Psi_{\boldsymbol{\varrho}}(\mathbf{X})$ are respectively the coefficient and the multivariate polynomial associated with the multi-index $\boldsymbol{\varrho}$. Details on how to find the multi-index, which are lists of natural numbers whose sum of terms is less than or equal to the degree of the selected polynomial can be found in (Sudret, 2014). The amount of terms in the multi-index is equal to the amount of random variable M, enabling $\boldsymbol{\varrho}$ to be written as

$$\boldsymbol{\varrho} = (\varrho_1, \varrho_2, \cdots, \varrho_M), \qquad \varrho_i \in \mathbb{N}. \tag{9}$$

Consequently, the multivariate polynomial is associated with multi-index $\boldsymbol{\varrho}$ as follows

$$\Psi_{\boldsymbol{\varrho}}(\boldsymbol{x}) \stackrel{\text{def}}{=} \prod_{i=1}^{M} \psi_{\varrho_i}^{(i)}(x_i), \tag{10}$$

where $\psi_{\varrho_i}^{(i)}$ is the univariate polynomial associated with the corresponding random variable and the index of the list of integers. Univariate polynomials are orthonormal polynomials which are dependent on the marginal distribution considered for the input random variable X_i. For instance, Hermite polynomials are used for normal distribution variables, while Legendre and Laguerre polynomials for uniform and gamma distributions, respectively. It is therefore important to standardize the input variables to be able to define the respective polynomial.

The sum of indexes represents the degree associated with the polynomial and is written as

$$|\boldsymbol{\varrho}| = \sum_{i=1}^{M} \varrho_i. \tag{11}$$

The set $\mathcal{A}^{M,p}$ with all possible multi-indices, whose sum of terms is lower than or equal to degree p of the selected polynomial, is represented as

$$\mathcal{A}^{M,p} = \{\boldsymbol{\varrho} \in \mathbb{N}^M \ \ |\boldsymbol{\varrho}| \leq p\}. \tag{12}$$

The number of bases in a polynomial with M random variable and degree p can be found by the following binomial

$$\text{card}\, \mathcal{A}^{M,p} = \binom{M+p}{p} = \frac{(M+p)!}{M!p!}. \tag{13}$$

Using this number, the polynomial represented in Eq. (8) can be truncated to

$$Y \approx \sum_{\boldsymbol{\varrho} \in A} c_{\boldsymbol{\varrho}} \Psi_{\boldsymbol{\varrho}}(\mathbf{X}). \tag{14}$$

The bases are determined by means of the probability distribution of each marginal variable and the multivariate polynomial found by Eq. (10). The coefficients of the PCE can be found using least-square minimization to find the argument which minimizes the expectation of the squared difference between the computational model and the truncated polynomial expressed in Eq. (14), such that

$$\boldsymbol{c} = \arg \min_{\boldsymbol{c} \in \mathcal{R}^{\text{card},\mathcal{A}}} \mathbb{E}\left[\left(\mathcal{M}(\mathbf{X}) - \sum_{\boldsymbol{\varrho} \in \mathcal{A}} c_{\boldsymbol{\varrho}} \Psi_{\boldsymbol{\varrho}}(\mathbf{X})\right)^2\right]. \tag{15}$$

The methodology then consists of drawing a random sample $\mathcal{X} = \{\boldsymbol{x}^{(i)},\ i = 1, \cdots, n\}$ by Monte Carlo Simulation (MCS), Latin Hypercube Sampling (LHS), Sobol or another method and estimating the response of the model

$$\mathcal{Y} = \{y^{(1)} = \mathcal{M}(\boldsymbol{x}^{(1)}), \cdots, \boldsymbol{y}^{(n)} = \mathcal{M}(\boldsymbol{x}^{(n)})\}^T. \tag{16}$$

A special matrix A is used to evaluate the bases of the PCE for each random sample as follows

$$\mathbf{A} = \{\mathbf{A}_{ij} \stackrel{\text{def}}{=} \Psi_j(\boldsymbol{x}^{(i)}),\ i = 1, 2, \cdots, n,\ j = 1, 2, \cdots, \text{card}(\mathcal{A})\}. \tag{17}$$

Then, the coefficients are estimated and stated as

$$\hat{\boldsymbol{c}} = (\mathbf{A}^T\mathbf{A})^{-1}\mathbf{A}^T\mathcal{Y}. \tag{18}$$

The mean and variance of the now stochastic response are estimated from the coefficients of the PCE as

$$\mu_{\hat{Y}} = \mathbb{E}[\hat{Y}] = \mathbb{E}[\sum_{\boldsymbol{\varrho} \in A} \hat{c}_{\boldsymbol{\varrho}} \Psi_{\boldsymbol{\varrho}}(\mathbf{X})] = c_0, \tag{19}$$

$$\sigma_{\hat{Y}}^2 \stackrel{\text{def}}{=} \text{Var}[\hat{Y}] = \mathbb{E}\left[(\hat{Y} - c_{\mathbf{0}})^2\right] = \sum_{\substack{\boldsymbol{\varrho} \in A \\ \boldsymbol{\varrho} \neq \mathbf{0}}} \hat{c}_{\boldsymbol{\varrho}}^2. \tag{20}$$

In the present case, the response function is defined as the power output FRF, evaluated at the input excitation frequency from Eq. (6). Based on a pre-defined stochastic model for the uncertain parameters, the PCE described above is used to estimate the resulting mean and variance of the power output.

4. ROBUST OPTIMIZATION USING COMPROMISE PROGRAMMING

Multi-objective optimization is common in engineering and different methods can be chosen according to the nature of the problem (Marler and Arora, 2004; Moreira, 2015). In addition, multi-objective optimization methods can be associated with a computational cost to converge towards the ideal solutions. Different from optimization with a single objective function, multi-objective optimization finds many solutions in a curve known as Pareto front. The solutions in this curve represent the ideal values and one goal cannot be modified without worsening other goal. Consequently, the construction method must be properly selected once the Pareto front for convex problems is different from that of non-convex problems. A well-known method to solve non-convex problems is known as Compromise Programming (CP) and its fundamental property is to minimize the norm of the difference between a function vector $f(\mathbf{x})$ and the vector of utopia point $\mathbf{u}$. Since $\mathbf{x}$ is a vector of parameters or design variables to be found, the following problem may be written (Chen *et al.*, 1998)

$$\begin{aligned} &\text{Minimize} \quad \|f(\mathbf{x}) - u\| = (\sum_{i=1}^{m} |f_i(\mathbf{x}) - u_i|^p)^{1/p}, \quad i = 1, 2, \cdots, m. \\ &\text{Subject to } \mathbf{x} \in X, \end{aligned} \tag{21}$$

where X is the space of design variables $\mathbf{x}$ and constraints while p is the index which defines the type of metric. For a weighted metric, the latter problem is rewritten as

$$\begin{aligned} &\text{Minimize} \quad (\sum_{i=1}^{m} w_i |f_i(\mathbf{x}) - u_i|^p)^{1/p} \\ &\text{Subject to } \mathbf{x} \in X, \end{aligned} \tag{22}$$

where w_i is positive with $\sum_{i=1}^{m} w_i = 1$. For $p = 1$, Wq. (22) represents the classical weighted sum (WS) method which solve many types of convex problems. The CP method considers a Tchebycheff metric such that $p = \infty$ and, thus, is able to solve non-convex problems. Then, the last optimization is expressed as a min-max problem such as

$$\min_{\mathbf{x} \in X} \max_{1 \leq i \leq m} w_i (f_i(\mathbf{x}) - u_i). \tag{23}$$

The min-max problem may be written as a β-problem as

$$\begin{aligned} &\text{Minimize} \quad \beta \\ &\text{Subject to} \quad w_i (f_i(\mathbf{x}) + \epsilon - \bar{f}_i) \leq \beta, \quad i = 1, 2, \cdots m. \\ &\qquad\qquad \mathbf{x} \in X, \end{aligned} \tag{24}$$

where $\epsilon \geq 0$ and $u_i = \bar{f}_i - \epsilon$.

The robust analyses using the mean value μ_f and the relative dispersion parameter $\delta_f = \sigma_f / \mu_f$, i.e the ratio between the standard deviation and the mean value, can be stated as a CP method such that a bi-objective optimization is defined and given by

$$\begin{aligned} &\text{Minimize} \quad \beta \\ &\text{Subject to} \quad w_1 \left(\frac{\mu_f}{\mu_f^\star} + \epsilon_1 - \bar{f}_1 \right) \leq \beta \\ &\qquad\qquad (1 - w_1) \left(\frac{\delta_f}{\delta_f^\star} + \epsilon_2 - \bar{f}_2 \right) \leq \beta \\ &\qquad\qquad \mathbf{x} \in X \end{aligned} \tag{25}$$

where $\mu_f^\star$ and $\delta_f^\star$ are the optimal values for the mean and relative dispersion, respectively. Thus, using the mean and variance estimated by Eqs. (19) and (20), the robust analyses may be performed by applying the CP method according to the problem given in Eq. (25).

5. ROBUST OPTIMIZATION USING NSGA-II

The Non-dominated Sorting Genetic Algorithm (NSGA-II) is a method based on the classical genetic algorithm to solve problems with different objective functions simultaneously. For this reason, a population of points in each run of the algorithm is chosen in order to converge towards the Pareto front. Different from the CP method where a weighted factor is selected to find a desired solution, in the NSGA-II, a population of points is available on the optimal Pareto front for

an appropriate choice *a posteriori*. Additionally, in the convergence procedure, the method seeks multiple non-dominated solutions assigning fitness to the population members and trying to ensure the diversity of points in the final solutions (Deb *et al.*, 2002).

In the genetic algorithm (GA), the convergence process is divided into stages of reproduction, crossover and mutation based on biological evolution concepts (Rao, 2009). The variables are manipulated using strings and a fitness function is evaluated to select the best strings. By means of probabilistic concepts, the best strings are selected at the reproduction stage and copies are created to form the mating pool. After this stage, part of the population from the mating pool is chosen and the crossover operator is applied by combining portions of the strings aiming at producing better fitness values. Finally, the mutation operator is implemented by modifying certain binary digits of the new strings according to a specified probability. The steps are repeated for each iteration to find the optimal design variable by minimizing/maximizing a specific function in the convergence process.

The stages presented in the genetic algorithm are used in the NSGA-II to find non-dominated solutions and to ensure the diversity in the population. Thus, the first procedure is to rank the individuals by dividing the solutions in fronts or ranks, which are chosen according to the dominance concept. This is done by considering a Pareto-optimal criteria such that one goal cannot be modified without worsening another goal. For instance, a hypothetical population can divided in rank 1, rank 2 and rank 3 so that the individuals of rank1 are closer to the optimum Pareto front and should be preferred in the non-dominance procedure. Then, for individuals in the same rank, the diversity of the population is preserved by considering solutions in a less crowded area with the help of an operator that measures the crowding distance.

The initial population with N individuals in NSGA-II is ranked and the operators of reproduction, crossover and mutation are applied to create an offspring population. The new population, which consists of $2N$ individuals, are sorted according to the dominance concept in the best ranks. Also, the crowding distance operator is applied to the individuals in the same rank. Hence, the population is truncated and the best solutions of N individuals are separated, ending the iteration. This process is repeated in order to find the Pareto-optimal solutions based on the number of iterations determined by the end-user.

6. DESIGN OF ROBUST ENERGY HARVESTING DEVICES

The design strategy for robust energy harvesting devices consists of: i) defining the design and uncertain parameters; ii) estimating the mean and variance of the power output FRF; and iii) applying the multi-objective optimization methods. Since dispersion is used for multi-objective optimization, the variance must be found previously. The vector of design parameters is defined as $\mathbf{x}_p = \{l_v, R_c, h_p, l_p/l_v, d_p/(l_v - l_p)\}$ according to Fig. 1. The variable l_p/l_v allow to find the length of the sensor l_p given the length of the substrate l_v, while with the variable $d_p/(l_v - l_p)$ it is possible to find the distance of the sensor relative to the clamp d_p. In the following, the uncertain parameters are chosen as the imperfect clamp linear k_w and torsional k_θ springs, the effective damping ζ of the device, and the effective electrical resistance R_c of the circuit. In this work, Gamma probability distribution functions (p.d.f.) are assumed for all uncertain variables, with shape parameter $\alpha = (\mu/\sigma)^2 = 1/\delta^2$ and scale parameter $\beta = \sigma^2/\mu = \mu\delta^2$. By defining the mean, standard deviation or dispersion values of each variable, the parameters α and β are found and the Gamma p.d.f. is determined for the uncertain variables. The FRF of power output indicated by Eq. (6) is evaluated for a given vector of design parameters $\mathbf{x}_p$ and excitation frequency ω such that

$$f(\boldsymbol{x}_p, \omega) = G_{P\ddot{w}_0}(\mathbf{x}_p, \omega). \tag{26}$$

As the purpose of the energy harvesting device design optimization is to maximize the harvested power output, the device resonance frequency must be tuned to the excitation frequency. This is done by internally evaluating the tip mass, through its height h_b, for a given set of device parameters so that the resonance frequency matches the pre-defined target frequency. Then, for each design parameters vector $\mathbf{x}_p$ and based on the stochastic models for the uncertain parameters vector $\boldsymbol{x} = \{k_w, k_\theta, \zeta, R_c\}$, the PCE procedure is applied to estimate the mean and variance of the harvested power output, using Eqs. (19) and (20), respectively. For the PCE calculations, a Latin Hypercube Sampling (LHS) with Monte Carlo Simulation (MCS) was used to sample the random variables in vector $\boldsymbol{x}$ that allows to estimate the model response and the PCE coefficients. All calculations are done using Matlab® software.

The utopia values $\mu_f^\star$ and $\delta_f^\star$ of Eq. (25) are found by maximizing the mean and minimizing the dispersion using genetic algorithm to solve the following deterministic problems

$$\begin{aligned} &\text{find} && \mathbf{x}_p \\ &\text{maximizing} && \mu_f \\ &&& \mathbf{x}_p^L \leq \mathbf{x}_p \leq \mathbf{x}_p^U \end{aligned} \tag{27}$$

$$\begin{aligned} &\text{find} && \mathbf{x}_p \\ &\text{minimizing} && \delta_f \\ &&& \mathbf{x}_p^L \leq \mathbf{x}_p \leq \mathbf{x}_p^U \end{aligned} \tag{28}$$

where $\mathbf{x}_p^L$ and $\mathbf{x}_p^U$ are the lower and upper bounds, respectively, for the design variables.

Next, the CP method is applied to find the vector of optimal robust design variables $\mathbf{x}_p$ for different weighting factors w_1 in Eq. (25). This allows to determine and plot a Pareto front for the different solutions found by modifying the weighting factor. In parallel, the NSGA-II method is also applied by considering mean and dispersion as objective functions without the need to compute utopia points as in the CP method. Hence, using only Eqs. (19) and (20) estimated by the PCE, the NSGA-II is applied to find the Pareto-optimal front according to a pre-defined number of devices (solutions). For both methods, a box plot is also plotted to analyze and compare nominal performance and variability of the obtained harvesting devices.

7. ROBUST DESIGN RESULTS

Based on an experimental setup used for verification and in reference to the device shown schematically in Fig. 2, the following nominal parameters were considered: distance between piezoelectric patch and clamp $d_p = 1.1$ mm, piezoelectric patch thickness $h_p = 0.13$ mm, substrate thickness $h_v = 1$ mm, adhesive layer thickness $h_a = 0.08$ mm, substrate length $l_v = 74.7$ mm, piezoelectric patch length $l_p = 73.6$ mm and considering also all parts with 12.8 mm of width. The tip mass, which has length and height of $l_b = h_b = 12.8$ mm, is on top of a segment of the substrate, thus the total mass is estimated at 9.2 g and rotation inertia at 0.8 kg mm^2. A PZT-5A piezoceramic was considered with elastic stiffness constant $\bar{c}_{11}^E = 66.3$ GPa, piezoelectric constant $\bar{e}_{31} = 13.3$ C/m^2 and dielectric constant $\bar{\epsilon}_{33}^{\bar{\epsilon}} = 12.3$ nF/m and density 7850 kg m^{-3}. For the substrate, aluminum was considered with Young's modulus 68 GPa and density 2700 kg m^{-3}. The Epoxy-based adhesive layer has Young's modulus 2 GPa and density 1126 kg m^{-3}. For verification purposes, the transmissibility FRFs of acceleration at the tip mass and voltage induced at the piezoelectric patch with respect to the base input harmonic displacement $w_0(t)$ were evaluated and compared to the corresponding FRFs obtained experimentally. They are shown in Figs. 3(a) and 3(b), respectively, for two values of resistance $R_c = 100$ kΩ and $R_c = 1000$ kΩ. The damping identified in the experimental tests of $\zeta = 1.1\%$ was also used in the numerical model.

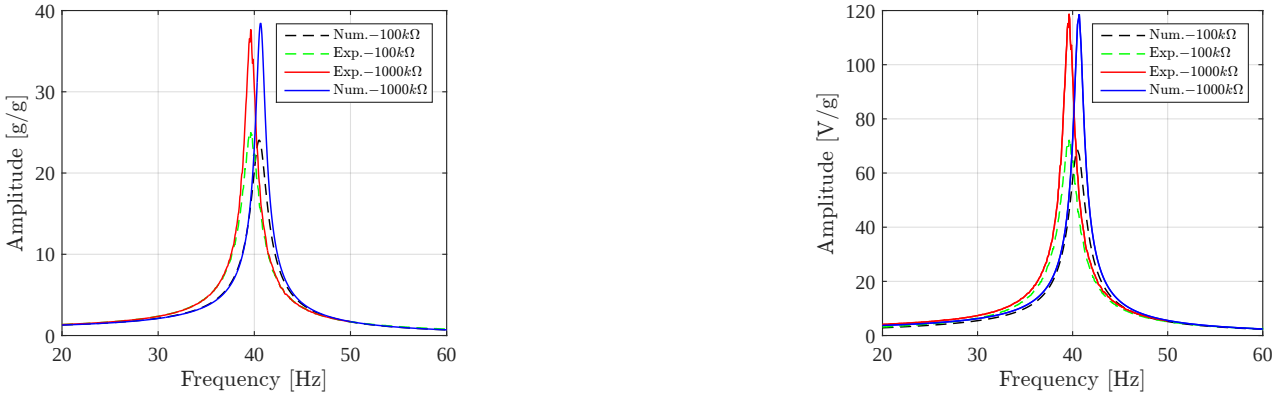

(a) FRF of acceleration output

(b) FRF of voltage output

Figure 3: Numerical and experimental FRFs for tip acceleration and voltage outputs.

Once the model was verified, the uncertain variables were chosen to perform the robust analyses. The mean values considered for the uncertain variables are $k_w = 50$ kN/m, $k_\theta = 0.3$ kNm/rad and $\zeta = 1.1\%$. For the electrical resistance R_c, the mean value is defined as the value in the design vector. The reason for this is that the electrical resistance is considered as both uncertain and design variables. Additionally, the relative tolerance for each variable k_w, k_θ, ζ and R_c was assumed to be 90%, 90%, 10% and 30%, respectively, and equal to three times the relative dispersion. For the design variables, the corresponding lower and upper limits were set as $\mathbf{x}_p^L = \{65\text{ mm},\ 20\text{ k}\Omega,\ 0.13\text{ mm},\ 0.8,\ 0\}$ and $\mathbf{x}_p^U = \{85\text{ mm},\ 400\text{ k}\Omega,\ 0.25\text{ mm},\ 0.97,\ 0\}$. The excitation frequency was set at 40 Hz, which is very close to the resonance frequency of the nominal device.

To estimate mean and variance, a PCE of degree 3 was selected and 400 samples were used with the MCS and LHS to calculate the PCE coefficients. For the CP optimization method, utopia points for mean $\mu_f^\star$ and dispersion $\delta_f^\star$ were found by solving the optimization problems defined in Eqs. (27) and (28), respectively. For that, a genetic algorithm search was selected with a probability of crossover and mutation of 90% and 30%, respectively, 50 individuals and 150 generations. This procedure led to $\mu_f^\star = 80.2$ mW/g^2, for $\mathbf{x}_p = \{65\text{ mm},\ 252.6\text{ k}\Omega,\ 0.25\text{ mm},\ 0.97,\ 0\}$, meaning $l_p = 0.97\, l_v = 63.05$ mm and $d_p = 0$, and $\delta_f^\star = 3.31\%$, for $\mathbf{x}_p = \{85\text{ mm},\ 63.4\text{ k}\Omega,\ 0.18\text{ mm},\ 0.8,\ 0\}$.

Then, the CP method was used to identify other devices using Eq. (25) with $\mu_f/\mu_f^\star = \delta_f/\delta_f^\star = 1$ such as $\bar{f}_1 = \bar{f}_2 = 1$ and $\epsilon_1 = \epsilon_2 = 0$. The modification of w_1 led to different optimal devices as indicated in Table 1, in which the values of the tip mass height h_b were included for completeness. By selecting higher weighting factors, devices with a higher $\mu_f/\mu_f^\star$

value can be designed, resulting in better nominal performance. On the other hand, smaller values of the ratio $\delta_f/\delta_f^\star$ means more robust devices and this occurs when w_1 is reduced in the optimization. Devices with shorter lengths, and thus larger tip mass heights, lead to better mean performance while devices with greater lengths are more robust. All designed devices had $d_p = 0$, that is, the sensor is attached to the clamp in all cases. Also, smaller relative piezoelectric patch length l_p/l_v values resulted in an increase in robustness, with a consequent loss of mean performance. With exception of the last device, which has a smaller patch thickness, all other devices had similar (maximum) thicknesses. The robustness also had a tendency to increase for smaller electrical resistance values.

Table 1: Devices and design variables obtained with the CP method.

Device	w_1	l_v (mm)	h_b (mm)	R_c (kΩ)	h_p (mm)	$\frac{l_p}{lv}$	$\frac{d_p}{l_v - l_p}$	$\frac{\mu_f}{\mu_f^\star}$	$\frac{\delta_f}{\delta_f^\star}$
#1	1	65.0	27.2	252.7	0.25	0.97	0	1.0	2.08
#2	0.9	65.0	26.7	107.9	0.25	0.96	0	0.95	1.57
#3	0.8	66.6	24.9	109.8	0.25	0.87	0	0.89	1.47
#4	0.7	68.9	23.1	123.0	0.25	0.85	0	0.85	1.41
#5	0.6	71.5	20.9	109.9	0.24	0.86	0	0.80	1.37
#6	0.5	73.3	19.6	119.5	0.25	0.87	0	0.77	1.30
#7	0.4	76.5	17.4	100.7	0.25	0.83	0	0.70	1.18
#8	0.3	79.1	15.9	97.9	0.25	0.82	0	0.66	1.12
#9	0.2	81.9	14.3	94.5	0.25	0.83	0	0.62	1.06
#10	0.1	84.5	13.0	94.1	0.25	0.81	0	0.57	1.02
#11	0	85.0	10.2	63.0	0.18	0.80	0	0.48	1.00

Figure 4 shows the FRF of power output per unit squared input acceleration for the devices described in Table 1, which are tuned at 40 Hz. Moreover, the Pareto front is depicted in Fig. 5(a) while Fig. 5(b) shows a box plot for each device with mean values and six standard deviations of tolerance. From the Pareto front, the designer or decision-maker may choose in a trade-off analysis between mean value and dispersion. From the box plot, is possible to verify that the first device generates more power, in mean terms, but the device 2 is more robust and, consequently, could possibly perform better in view of uncertainties. From Table 1, this occurs by mainly reducing the electrical resistance, because the change in l_p/l_v was minimal. Each device in Fig. 5(b) can also be compared with its successor or predecessor in terms of upper and lower bounds. For instance, device 2 may be better than device 1 since, in a worst case scenario, the minimum power generated by device 2 is superior to the one of device 1. On the other hand, device 2 is always better than the device 11 since the worst case for device 2 is still better than the best case for device 11.

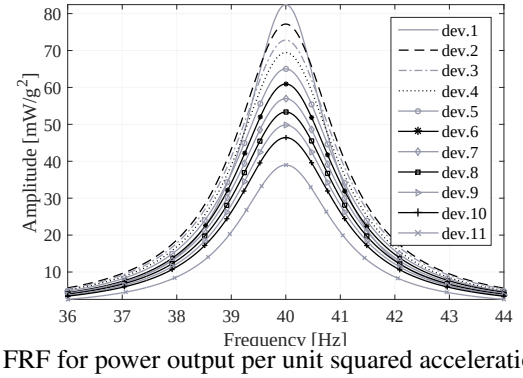

Figure 4: FRF for power output per unit squared acceleration input.

The same procedure was performed using the NSGA-II method, with the advantage that the mean and dispersion functions can be used directly in the optimization. In this case, 30 individuals and 500 generations were chosen with crossover and mutation rates of 70% and 30%, respectively. The obtained Pareto front is represented in Fig. 6(a) for 30 individuals. Eleven devices were selected for comparison with the CP method, which are marked with a cross in Pareto-front. These devices are shown in Table 2 and in the box plot represented in Fig. 6(b). The box plot shows that devices 2 up to 4 may be better than device 1 and this occurs by decreasing the electrical resistance, according to the parameters shown in Table 2, since l_p/l_v alters imperceptibly. Other devices can be compared in the same manner as in the CP method. In terms of performance and robustness, and for both methods, the device may be selected based on a subjective choice of the decision-maker, using the Pareto-front and box plot analyses.

Pareto-fronts were found using both optimization methods investigated, but more devices were found using NSGA-II.

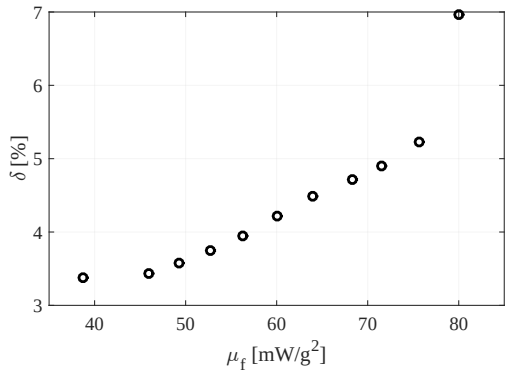

(a) Pareto-front for dispersion and mean power

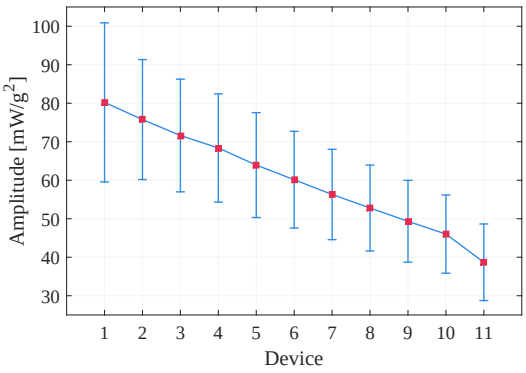

(b) Box plot of power generated for each device

Figure 5: Pareto-front and box plot of power generated for each device considering $+/-3\sigma$ based on CP method.

Table 2: Selected devices and design variables obtained with the NSGA-II method.

Device	l_v (mm)	h_b (mm)	R_c (kΩ)	h_p (mm)	$\frac{l_p}{l_v}$	$\frac{d_p}{l_v - l_p}$	μ_f (mW/g^2)	δ_f (%)
#1	65.0	27.2	246.2	0.25	0.97	0	80.22	6.81
#2	65.0	27.1	218.4	0.25	0.96	0	79.83	6.42
#3	65.0	27.0	173.0	0.25	0.96	0	78.65	5.86
#4	65.0	26.8	138.3	0.25	0.95	0	76.87	5.41
#5	66.1	25.6	125.9	0.25	0.91	0	73.88	5.10
#6	68.9	23.0	108.4	0.25	0.90	0	68.75	4.70
#7	69.9	21.8	101.1	0.24	0.85	0	65.30	4.32
#8	74.1	19.0	96.7	0.25	0.86	0	59.95	3.89
#9	78.4	15.9	90.3	0.24	0.84	0	52.89	3.74
#10	82.7	13.9	102.2	0.25	0.84	0	48.73	3.54
#11	85.0	12.1	80.1	0.23	0.81	0	43.69	3.33

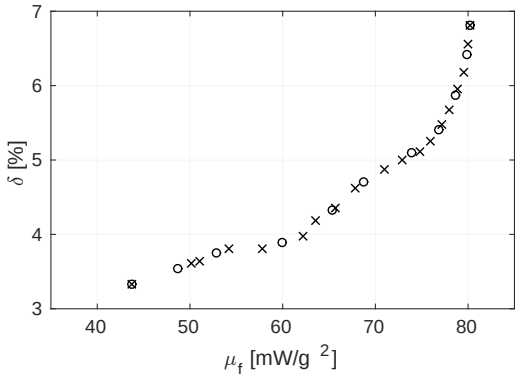

(a) Pareto-front for dispersion and mean power

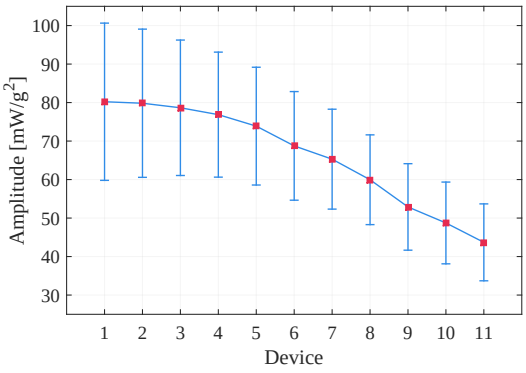

(b) Box plot of power generated for each device

Figure 6: Pareto-front and box plot of power generated for each device considering $+/-3\sigma$ based on NSGA-II.

Also, NSGA-II needs only a single run with 30 individuals while the CP method required eleven runs to yield eleven devices. On the other hand, the most robust device was found in the CP method while in NSGA-II this fact did not occur with 30 individuals. To find a diversity of points in Pareto-front, more individuals are needed, while in the CP method modifying manually the weighting factor, a specific device can always be found in terms of mean and dispersion.

8. CONCLUSION

This work presented some recent results on the robust design of energy harvesting devices, based on cantilever resonating beams, when subjected to uncertainties on the beam clamping, harvesting circuit and effective damping. Multi-

objective optimization techniques, CP and NSGA-II, were applied to search for optimal values of design parameters, namely beam length, piezoeletric patch length, position and thickness and circuit effective resistance, leading to satisfactory compromises between mean and dispersion of the potentially harvested energy. For that, the mean and variance of the harvested power output were estimated using polynomial chaos expansions and the relative dispersion was used to quantify a device's robustness. Results have shown that harvesting devices with smaller length and larger masses generally lead to best nominal performance but also to higher dispersions. Also, the dispersions can be reduced by using effective circuit resistances smaller than the nominal values. Several design alternatives were presented in the form of a Pareto front, from which a designer can choose based on the desired compromise.

ACKNOWLEDGEMENTS

Support of CNPq, grants 309193/2014-1 and 309001/2018-8, and CAPES doctoral scholarship, is acknowledged.

REFERENCES

Beyer, H.S. and Sendhoff, B., 2007. "Robust optimization–a comprehensive survey". *Computer methods in applied mechanics and engineering*, Vol. 196, No. 33-34, pp. 3190–3218.

Chen, W., Wiecek, M.M. and Zhang, J., 1998. "Quality utility: a compromise programming approach to robust design". In *International Design Engineering Technical Conferences and Computers and Information in Engineering Conference*. American Society of Mechanical Engineers, Vol. 80326, p. V002T02A032.

Coello, C.A.C., Pulido, G.T. and Lechuga, M.S., 2004. "Handling multiple objectives with particle swarm optimization". *IEEE Transactions on evolutionary computation*, Vol. 8, No. 3, pp. 256–279.

De Marqui Junior, C., Erturk, A. and Inman, D.J., 2009. "An electromechanical finite element model for piezoelectric energy harvester plates". *Journal of Sound and Vibration*, Vol. 327, No. 1-2, pp. 9–25.

Deb, K., Pratap, A., Agarwal, S. and Meyarivan, T., 2002. "A fast and elitist multiobjective genetic algorithm: Nsga-ii". *IEEE transactions on evolutionary computation*, Vol. 6, No. 2, pp. 182–197.

Dutoit, N.E., Wardle, B.L. and Kim, S.G., 2005. "Design considerations for mems-scale piezoelectric mechanical vibration energy harvesters". *Integrated ferroelectrics*, Vol. 71, No. 1, pp. 121–160.

Erturk, A. and Inman, D.J., 2011. *Piezoelectric energy harvesting*. John Wiley & Sons.

Franco, V.R. and Varoto, P.S., 2017. "Parameter uncertainties in the design and optimization of cantilever piezoelectric energy harvesters". *Mechanical Systems and Signal Processing*, Vol. 93, pp. 593–609.

Godoy, T.C. and Trindade, M.A., 2012. "Effect of parametric uncertainties on the performance of a piezoelectric energy harvesting device". *Journal of the Brazilian Society of Mechanical Sciences and Engineering*, Vol. 34, pp. 552–560.

Godoy, T.C., Trindade, M.A. and Deü, J.F., 2014. "Topological optimization of piezoelectric energy harvesting devices for improved electromechanical efficiency and frequency range". In *Proceedings of 10th World Congress on Computational Mechanics (WCCM), São Paulo*. pp. 4003–4016.

Kim, J., Lee, T.H., Song, Y. and Sung, T.H., 2017. "Robust design optimization of fixed-fixed beam piezoelectric energy harvester considering manufacturing uncertainties". *Sensors and Actuators A: Physical*, Vol. 260, pp. 236–246.

Kim, M., Hoegen, M., Dugundji, J. and Wardle, B.L., 2010. "Modeling and experimental verification of proof mass effects on vibration energy harvester performance". *Smart Materials and Structures*, Vol. 19, No. 4, p. 045023.

Lee, K.H. and Park, G.J., 2006. "A global robust optimization using kriging based approximation model". *JSME International Journal Series C Mechanical Systems, Machine Elements and Manufacturing*, Vol. 49, No. 3, pp. 779–788.

Leo, D.J., 2007. *Engineering analysis of smart material systems*, Vol. 435. Wiley Online Library.

Lobato, F.S., 2008. *Multi-objective Optimization for Engineering System Design (in portuguese)*. Ph.D. thesis, Federal University of Uberlândia.

Marler, R.T. and Arora, J.S., 2004. "Survey of multi-objective optimization methods for engineering". *Structural and multidisciplinary optimization*, Vol. 26, No. 6, pp. 369–395.

Moreira, F.R., 2015. *Robust Optimization Multiobjective for Engineering System Design (in portuguese)*. Ph.D. thesis, Federal University of Uberlândia.

Rao, S.S., 2009. *Engineering optimization: theory and practice*. John Wiley & Sons.

Ruiz, R.O. and Meruane, V., 2017. "Effect of uncertainties in the dynamical behavior of piezoelectric energy harvesters". *Procedia engineering*, Vol. 199, pp. 3486–3491.

Santos, H.F.L., 2008. *Structural vibration control using piezoceramics in extension and shear connected to hybrid active-passive circuits (in portuguese)*. Master's thesis, University of São Paulo.

Schuëller, G.I. and Jensen, H.A., 2008. "Computational methods in optimization considering uncertainties–an overview". *Computer Methods in Applied Mechanics and Engineering*, Vol. 198, pp. 2–13.

Sudret, B., 2014. *Polynomial chaos expansions and stochastic finite element methods*. CRC Press, chapter 6, pp. 265–300.

RESPONSIBILITY NOTICE

The authors are solely responsible for the printed material included in this paper.